

# Engineered a novel polyoxometalates-based composite platform with pH-responsive selectivity for efficient and controllable separation of ovalbumin and lysozyme from complex egg white sample

Qian Sun<sup>a,1</sup>, Yujing Wang<sup>a,1</sup>, Ye Wang<sup>a</sup>, Guangtian Zhu<sup>a</sup>, Yifei Niu<sup>a</sup>, Weizhu Wang<sup>c</sup>, Ronghua Fan<sup>b,\*</sup>, Dandan Zhang<sup>a,\*</sup>

<sup>a</sup> Liaoning Medical Functional Food Professional Technology Innovation Center, School of Public Health, Shenyang Medical College, Shenyang 110034, China

<sup>b</sup> Department of Sanitary Inspection, School of Public Health, Shenyang Medical College, Shenyang 110034, China

<sup>c</sup> Second Clinical Medical School, Shenyang Medical College, Shenyang 110034, China

## ARTICLE INFO

### Keywords:

Polyoxometalates  
Ovalbumin  
Lysozyme  
Isolation and purification

## ABSTRACT

This study aimed to engineer a novel polyoxometalates composite for efficient and controllable separation of ovalbumin (Ova) and lysozyme (Lys) from complex egg white sample. Here, we synthesized the SbW<sub>9</sub>@PEI composite via liquid-phase method with pH-responsive selectivity. At pH 4.0, the composite (2 mg) achieved 96 % adsorption efficiency for Ova (100 μg mL<sup>-1</sup>, 1 mL), with the adsorption capacity of 266.5 mg g<sup>-1</sup>. At pH 11.0, it exhibited 100 % adsorption efficiency for Lys (100 μg mL<sup>-1</sup>, 1 mL), with the adsorption capacity of 366.3 mg g<sup>-1</sup>. This method was successfully applied to the selective isolation of Ova and Lys from egg white, with the separated proteins being confirmed to have high purity. Notably, compared with untreated egg white, 10 and 40 low-abundance proteins were respectively identified through the separation of Ova and Lys. This study holds significant importance for the fields of functional food development, and food safety, et al.

## 1. Introduction

Eggs including egg white and yolk are a simple and nutritious cooking ingredient that is widely used in human diets and food processing. Egg white contains various proteins, including ovalbumin (Ova), ovotransferrin (Ovt), ovomucin, ovomucoid, and lysozyme (Lys) (Gazme, Rezaei, & Udenigwe, 2022). Due to the abundance of hydrophobic residues and free sulfhydryl groups in its structure, Ova has shown exceptional functional characteristics. Its high nutritional value, accessibility, and biocompatibility/biodegradability make Ova a potent candidate for food applications, such as being used as a gel forming agent, an emulsifier and a foam stabilizer, et al. (Rostamabadi et al., 2023). For example, Rao utilized an oil-in-water method to create the ovalbumin-carvacrol complex, which could effectively inhibit bacterial growth at lower concentrations and remained stable without degradation by light during storage. These complexes could serve as antimicrobial delivery systems in various food applications to combat foodborne pathogens (Rao et al., 2020). Liu successfully prepared Pickering emulsions stabilized by quercetin-ovalbumin composite

nanoparticles, demonstrating excellent emulsion stability during storage and significantly superior antimicrobial properties. Furthermore, the value of the emulsions in the application of food preservation was studied through its influence on the quality of fresh pork. As a novel food preservative, quercetin-ovalbumin composite nanoparticles show extremely broad application prospects (Liu et al., 2025). Lys is composed of a single polypeptide chain with 129 amino acids with a molecular weight of 14.3 kDa. It has demonstrated strong inhibitory effects against bacteria, fungi, and viruses, including the ability to prevent Norovirus contamination in food, making it a natural preservative for controlling bacterial growth in food products (Yang & Yan, 2025). Moreover, Lys is utilized in various cheese types to prevent late blowing caused by the fermentation of lactate by *Clostridium tyrobutyricum* (D'Incecco et al., 2016). Extensive research has been conducted on Lys due to its unique biological functions. For example, Niu prepared lysozyme-N-succinyl chitosan by using N-succinyl chitosan loaded lysozyme. Based to the high bacteriostatic activity of lysozyme-N-succinyl chitosan, the compound was used as bacteriostatic materials in strawberry preservation. This research provides a safe and feasible

\* Correspondence authors.

E-mail addresses: [fanronghua@symc.edu.cn](mailto:fanronghua@symc.edu.cn) (R. Fan), [zhangdandan@symc.edu.cn](mailto:zhangdandan@symc.edu.cn) (D. Zhang).

<sup>1</sup> These authors contributed equally: Qian Sun and Yujing Wang.

<https://doi.org/10.1016/j.foodchem.2025.146122>

Received 22 April 2025; Received in revised form 11 August 2025; Accepted 25 August 2025

Available online 26 August 2025

0308-8146/© 2025 Elsevier Ltd. All rights are reserved, including those for text and data mining, AI training, and similar technologies.

green bacteriostatic preservative material for the fresh storage of food (Niu, Zhu, Xi, Guo, & Wang, 2020). D'Incecco investigated the effects of Lys on lactic acid bacteria and free amino acids in 16 raw-milk hard cheeses produced in eight parallel cheese makings at four dairies. The results indicated that the addition of Lys encouraged the microbial degradation of arginine in the cheeses (D'Incecco et al., 2016). Furthermore, studies have shown that stomach lysozyme functions as a major digestive enzyme in ruminant-like mammals, helping to make those bacteria which enter the stomach from the foregut available for hydrolysis by conventional digestive enzymes (Dobson, Prager, & Wilson, 1984). Thus, the isolation and purification of Ova and Lys holds significant importance for the fields of functional food development, and food safety, et al.

Currently, there are several techniques available for isolating and purifying proteins from complex samples, such as ultrafiltration and affinity chromatography (Liu et al., 2020). Ultrafiltration uses pressure or centrifugal force to filter out solutes through a membrane for purification. It is effective for separating proteins with similar molecular weights but has drawbacks like low resolution and high impurity content (Wang et al., 2024). Affinity chromatography purifies proteins using biological molecule interactions, but faces challenges like non-specific binding, expensive affinity ligands, limited availability of suitable ligands, time-consuming optimization, and loss of target proteins during elution (Bilkova et al., 2025). Therefore, the development of efficient and selective methods for isolating and purifying Ova and Lys is crucial.

Polyoxometalates (POMs) are a class of ionic clusters formed by transition metal oxides connected through oxygen bridges. They have well-defined molecular structures include Keggin, Dawson, Anderson, and Waugh structures, with Keggin-type POMs being the most commonly used (Omwoma, Gore, Ji, Hu, & Song, 2015) and unique chemical properties, such as excellent redox characteristics, large size, high negative charge, nucleophilicity, and thermal stability (Li, Hu, Sa, & Feng, 2014; Yan et al., 2012). In addition, the cage-like structures of POMs allow them to form supramolecular compounds by binding with inorganic molecules, organic molecules, or ions. Therefore, they are widely used in catalysis, pharmaceuticals, electrochemistry, photochromism, magnetism, medicine, and more (Lv et al., 2022; Salazar Marcano, Lentink, Moussawi, & Parac-Vogt, 2021; Taheri, 2021; Wang et al., 2022). What is more worth mentioning is that the negative charge of polyoxometalates and the abundant oxygen atoms on their surfaces provide many effective binding sites for their interaction with proteins. Thus, the utilization of polyoxometalates composite in protein separation and purification is based on strong foundations, providing good selectivity, reusability, and high adsorption capacity, and more. For example, Zhang successfully synthesized a polyoxometalates composite,  $\text{Fe}_3\text{O}_4@PEI@POM1$ , with high adsorption selectivity and adsorption capacity, which effectively separated and purified IgG heavy chain and light chain from human serum (Zhang et al., 2018). Chen developed a hybrid TPPA-PMO<sub>12</sub> using polyoxometalates for the selective separation of  $\beta$ -lactoglobulin from complex samples, demonstrating efficient reusability (Chen, Zhang, Wang, Chen, & Wang, 2015).

Polyoxometalates  $\text{Na}_9[\text{SbW}_9\text{O}_{33}]\cdot 19.5\text{H}_2\text{O}$  ( $\text{SbW}_9$ ) belongs to the Keggin structure, but it differs from the classic Keggin structure. Due to the presence of a lone pair of electrons in the central atom Sb, it cannot form a central tetrahedral configuration with four coordination like P or Si to achieve a 1:12 saturated configuration, instead, it forms a tri-coordinated configuration, resulting in a 1:9 configuration (Bösing, Loose, Pohlmann, & Krebs, 2006; Han et al., 2016; Zhang et al., 2009). For the above reason, the number of structural variations in antimonytungstates is relatively limited. Currently reported antimonytungstates typically consist of two configurations:  $\alpha$ -type and  $\beta$ -type. Cai reported the first rare-earth cluster compound in POMs derivatives containing both  $\text{Sb}^{3+}$  and  $\text{Sb}^{5+}$ . Additionally, an effective and satisfactory ion strength control strategy was employed to modulate the structure and magnetic properties of the POMs material (Cai, Ye, Liu,

Guo, & Qiao, 2020). Sun synthesized a hexameric  $\beta$ - $[\text{SbW}_9\text{O}_{33}]^{9-}$  type antimonytungstate through a hydrothermal synthesis method and demonstrated its excellent proton conductivity (Sun et al., 2023). Gong (Gong, Wang, Zhao, & Yang, 2024) published a study on a novel antimonytungstate (AT)-based heterometallic framework biosensors. The article showed that the synthesized material can sensitively detect the KRAS gene (a key genetic marker for identifying the occurrence of malignant tumors), establishing a new platform for KRAS gene biosensing. It is precisely because of the rich structure of antimonytungstates and their high catalytic properties that they have many potential applications in various fields.

Consequently, the application of POMs in separating and purifying Ova and Lys has a good foundation. By designing simple and easy-to-operate synthesis methods to prepare POMs composite with pH-responsive selectivity and good adsorption performance, it is expected to use for the efficient and controllable separation of Ova and Lys from egg whites. This advancement will hold significant importance for the fields of functional food development, and food safety, et al. In this study, a new type of polyoxometalates composite,  $\text{SbW}_9@PEI$ , was prepared by grafting hyperbranched polyethyleneimine (PEI) onto polyoxometalates ( $\text{SbW}_9$ ) through electrostatic interaction. Comprehensive characterization confirmed the successful synthesis of the composite, elucidating the composite's chemical composition and morphology, et al. Utilizing the composite as a solid-phase adsorbent, we investigated the effects of pH, salt concentration, and time on the selective separation of the target proteins, explored the interaction mechanism between the composite and the proteins, and studied adsorption kinetics and adsorption isotherm models. Finally, the prepared  $\text{SbW}_9@PEI$  composite was applied to the controlled separation of Ova and Lys from complex egg white samples. The sodium dodecyl sulfate-polyacrylamide gel electrophoresis (SDS-PAGE) and liquid chromatography-tandem mass spectrometry (LC-MS/MS) were employed to assess the practical applicability performance of the composite.

## 2. Materials and methods

### 2.1. Chemicals and reagents

Ova, Lys and PEI were obtained from Sigma-Aldrich (St. Louis, USA). Coomassie Brilliant Blue G-250, sodium tungstate dihydrate ( $\text{Na}_2\text{WO}_4\cdot 2\text{H}_2\text{O}$ ) and hexadecyltrimethylammonium bromide (CTAB) were purchased from Sinopharm Chemical Reagent Co., Ltd. (Shanghai, China). Antimony (III) oxide was bought from Macklin Co., Ltd. (Shanghai, China). The protein molecular weight marker, sodium dodecyl sulfate (SDS), Glycine (Gly), and Tris (hydroxymethyl) amino-methane (Tris) were bought from Labgic Technology Co., Ltd. (Beijing, China). All the mentioned reagents were of analytical grade and used as received. Deionized water with a resistivity of 18 M $\Omega$  cm was used for all experiments.

### 2.2. Instrumentations

Fourier transform infrared (FT-IR) spectra were acquired using a Nicolet 6700 with wavenumbers ranging from 400 to 4000  $\text{cm}^{-1}$  (Thermo Fisher Nicolet, USA). Thermogravimetric analysis (TGA) was performed on a TGA/DSC 3+ analyzer (Mettler Toledo Company, Switzerland) at a heating rate of 10  $^\circ\text{C min}^{-1}$  under nitrogen atmosphere. X-ray Diffraction (XRD) patterns were measured on a D8 advance 2500 (Bruker, Germany) diffractometer, with XRD intensity data collected in the range of  $2\theta$  from  $5^\circ$  to  $80^\circ$  at room temperature. Scanning electron microscopy (SEM) images were captured using a Hitachi SU8020 scanning electron microscope (Hitachi, Japan), and energy X-ray dispersive (EDS) analysis was performed using a HORIBA EX350 (HORIBA Scientific, Ltd., France).  $\text{N}_2$  adsorption-desorption isotherm was measured by ASAP 2020HD88 BET analyzer (Micromeritics, USA). Transmission electron microscopy (TEM) images were

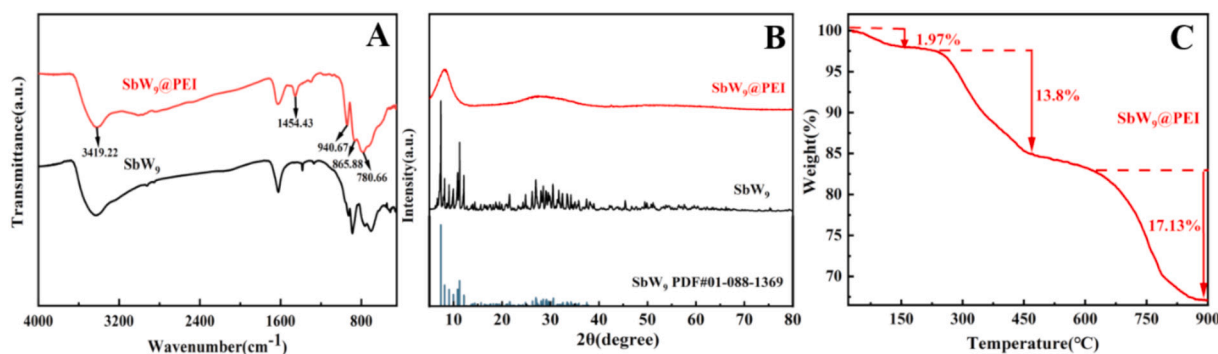


Fig. 1. (A) FT-IR spectra, (B) XRD of  $\text{SbW}_9$  and  $\text{SbW}_9@PEI$ , and (C) TGA curve of  $\text{SbW}_9@PEI$ .

taken on HITACHI H7650 transmission electron microscope (Hitachi, Japan). X-ray photoelectron spectroscopy (XPS) was conducted using the ESCALAB 250Xi Surface analysis system (Thermo Electron, England). Zeta potential measurement for surface charge analysis was performed by Zetasizer Nano ZS90 (Malvern, UK). The LC-MS/MS analysis was performed using an Easy nano-LC 1000 system (Thermo Fisher Scientific, Germany) interfaced with a Q Exactive Orbitrap mass spectrometer (Thermo Fisher Scientific, Germany).

### 2.3. Preparation of the $\text{SbW}_9@PEI$ composite

$\text{SbW}_9$  was prepared following the procedure outlined in the literature (Bösing et al., 2006). The specific steps were as follows. First, the  $\text{Na}_2\text{WO}_4 \cdot 2\text{H}_2\text{O}$  (40 g, 121 mmol) was dissolved in 80 mL of water. After the  $\text{Na}_2\text{WO}_4 \cdot 2\text{H}_2\text{O}$  solution reached boiling, the  $\text{Sb}_2\text{O}_3$  (1.96 g, 6.72 mmol) dissolved concentrated HCl (10 mL, 37 %) was added dropwise. The mixture underwent reflux for 1 h before being left to cool slowly. The colorless crystals of  $\text{SbW}_9$  appeared upon evaporation of one-third of the solution volume.

The  $\text{SbW}_9@PEI$  composite was prepared as follows:  $\text{SbW}_9$  (2.0 g) was dispersed in ultrapure water (30 mL) with vigorous stirring until a homogeneous transparent solution was obtained. Aqueous PEI solution (5 mL, 100 mg  $\text{mL}^{-1}$ ) was then introduced dropwise into the mixture under continuous magnetic stirring. Following a 7-h reaction at room temperature, the white precipitate that formed was recovered through centrifugation (8000 rpm, 10 min). The precipitate was then washed extensively with deionized water to eliminate any remaining unreacted materials, and finally dried in a vacuum oven at 60 °C for 36 h to obtain the  $\text{SbW}_9@PEI$  composite.

### 2.4. Adsorption/desorption of proteins by $\text{SbW}_9@PEI$ composite

In this experiment, the performance of  $\text{SbW}_9@PEI$  for protein adsorption was evaluated using Ova and Lys as protein models. The medium's pH was adjusted through hydrochloric acid and sodium hydroxide solutions. 2.0 mg of  $\text{SbW}_9@PEI$  was added to 1 mL of standard protein solutions with a concentration of 100  $\mu\text{g mL}^{-1}$ . The mixture was agitated for 10 min at room temperature to aid in the adsorption process, and then centrifuged at 8000 rpm for 5 min. The supernatant was collected to measure residual proteins by monitoring the absorbance at 595 nm using a UV-visible spectrophotometer after binding with Coomassie Brilliant Blue (Bradford method). The experiment's protein adsorption efficiency (E) was calculated using Eq. (1), where  $C_0$  represented the original protein concentration and  $C_1$  represented the residual protein concentration after adsorption.

$$E = \frac{C_0 - C_1}{C_0} \times 100\% \quad (1)$$

Kinetic adsorption experiments were performed by incubating 2 mg of  $\text{SbW}_9@PEI$  composite with 1 mL of protein solution (100  $\mu\text{g mL}^{-1}$ )

under controlled conditions. The adsorption process was monitored at room temperature with shaking time intervals of 5, 10, 15, 20, 25, 30, 35, 40, and 45 min. Following each incubation period, the mixture was centrifuged (8000 rpm, 5 min) to achieve phase separation, and the supernatant was carefully collected for subsequent analysis. The equilibrium concentration ( $C_e$ ) and adsorption capacity ( $q_e$ ) of protein were determined spectrophotometrically. The kinetic data were analyzed using three distinct models: the pseudo-first-order (PFO), pseudo-second-order (PSO), and Elovich equations, to elucidate the underlying adsorption mechanisms.

Adsorption isotherm experiments were conducted by adding 2 mg of  $\text{SbW}_9@PEI$  into separate centrifuge tubes containing 1 mL of protein solutions with varying concentrations (100–1500  $\mu\text{g mL}^{-1}$ ). After 10 min of shaking at room temperature, the mixtures were centrifuged at 8000 rpm for 5 min to achieve phase separation. The equilibrium concentration ( $C_e$ ) and adsorption capacity ( $q_e$ ) of protein were determined spectrophotometrically. The data were analyzed using six distinct models: Langmuir, Freundlich, Sips, Redlich, Temkin and Dubinin model.

The elution of Ova and Lys adsorbed on  $\text{SbW}_9@PEI$  could be effectively achieved using Tris-HCl (2 mol  $\text{L}^{-1}$ , pH = 9) and CTAB (0.01 mol  $\text{L}^{-1}$ ) solutions. The specific elution process involved mixing 1.0 mL of the elution agents with the composite after protein adsorption, shaking for 10 min, centrifuging at 8000 rpm for 5 min, measuring the absorbance value of the supernatant, and calculating the elution efficiency using the formula (2). The elution efficiency ( $E'$ ) of Ova and Lys was calculated based on the initial concentration ( $C_0$ ), the concentration after adsorption ( $C_1$ ), and the concentration after elution ( $C_2$ ).

$$E' = \frac{C_2}{C_0 - C_1} \times 100\% \quad (2)$$

### 2.5. Isolation of ovalbumin and lysozyme from egg white

Fresh eggs were purchased from the local market, after which the egg white and yolk were separated. Next, the egg white was diluted 300-fold and adjusted to pH 4 for Ova adsorption and pH 11 for Lys adsorption. To this diluted matrix, 0.3 mL of Lys standard solution (100  $\mu\text{g mL}^{-1}$ ) was spiked. The suspension was centrifuged (6000 rpm, 5 min) to remove insoluble particulates, retaining the supernatant for subsequent adsorption experiments. For protein adsorption, 2.0 mg of  $\text{SbW}_9@PEI$  composite was oscillated for 10 min with 1 mL of the above supernatant. After protein adsorption,  $\text{SbW}_9@PEI$  composite with adsorbed proteins was collected by centrifugation (8000 rpm, 5 min), washed twice with deionized water ( $2 \times 500 \mu\text{L}$ ), and then the adsorbed Ova and Lys were eluted by adding 300  $\mu\text{L}$  of elution solution (pH 9.0, 2 mol  $\text{L}^{-1}$  Tris-HCl, 0.01 mol  $\text{L}^{-1}$  CTAB) followed by vigorous shaking at 25 °C for 10 min. The eluate was collected after final centrifugation (8000 rpm, 5 min) and immediately analyzed by SDS-PAGE and LC-MS/MS.

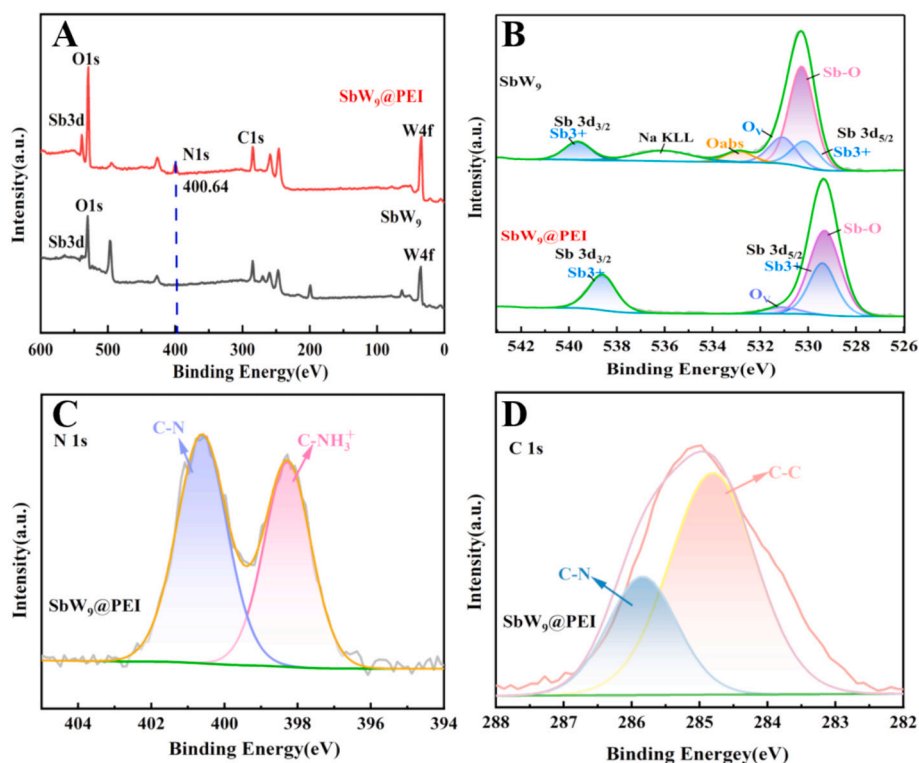


Fig. 2. (A) XPS spectra of  $\text{SbW}_9$  and  $\text{SbW}_9@\text{PEI}$ , (B) High-resolution Sb 3d XPS spectra of  $\text{SbW}_9$  and  $\text{SbW}_9@\text{PEI}$ , High-resolution (C) N 1s and (D) C 1s XPS spectra of  $\text{SbW}_9@\text{PEI}$ .

### 3. Results and discussion

#### 3.1. Characterizations of $\text{SbW}_9@\text{PEI}$ composite

The FT-IR spectra of  $\text{SbW}_9$  and  $\text{SbW}_9@\text{PEI}$  were presented in Fig. 1A. For  $\text{SbW}_9$ , the characteristic vibrational bands of the Keggin-type polyoxometalates structure were observed at  $926\text{ cm}^{-1}$  ( $\nu(\text{W}=\text{O}_t)$ ),  $889$

$\text{cm}^{-1}$  ( $\nu(\text{Sb}-\text{O}_a)$ ),  $767\text{ cm}^{-1}$  ( $\nu(\text{W}-\text{O}_b-\text{W})$ ), and  $704\text{ cm}^{-1}$  ( $\nu(\text{W}-\text{O}_c-\text{W})$ ), consistent with previous reports (Sun et al., 2023). In contrast, the spectrum of  $\text{SbW}_9@\text{PEI}$  not only retained these Keggin-related peaks but also exhibited new absorption bands at  $3419\text{ cm}^{-1}$  and  $1454\text{ cm}^{-1}$ , corresponding to the N—H stretching vibration and C—N stretching vibration of PEI, respectively. These findings confirmed the successful surface functionalization of  $\text{SbW}_9$  with PEI.

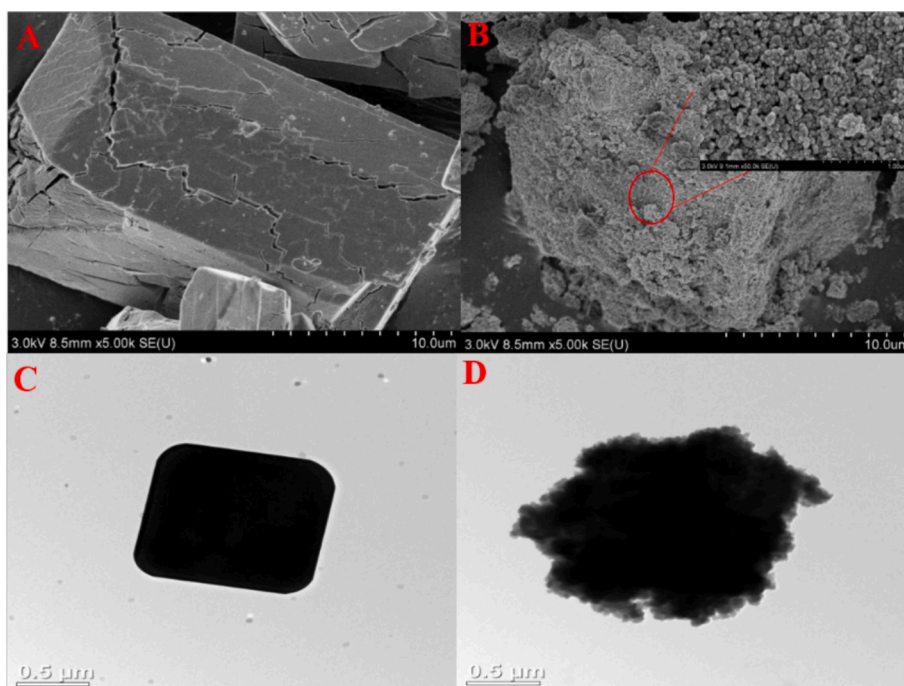


Fig. 3. (A, B) SEM images and (C, D) TEM images of  $\text{SbW}_9$  and  $\text{SbW}_9@\text{PEI}$ .

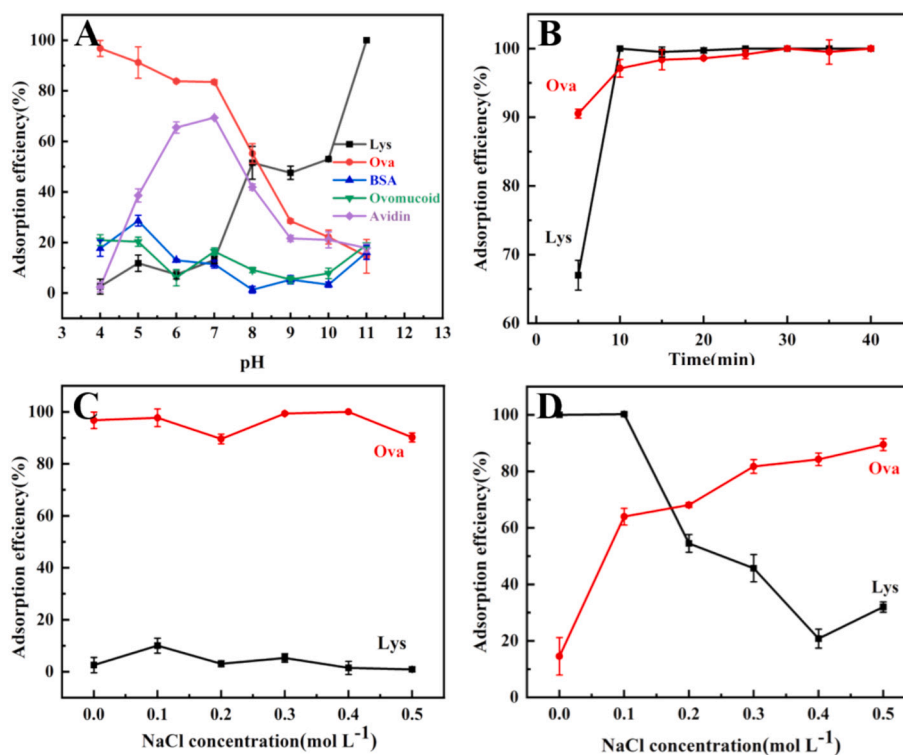


Fig. 4. (A) pH-dependent adsorption behaviors of proteins onto SbW<sub>9</sub>@PEI. Effect of (B) adsorption time, (C) the ionic strength at pH 4.0, (D) the ionic strength at pH 11.0 on the adsorption efficiency of Ova and Lys.

The XRD patterns of SbW<sub>9</sub> and SbW<sub>9</sub>@PEI were presented in Fig. 1B. The diffraction peaks of pristine SbW<sub>9</sub> matched well with the standard reference (PDF#01-088-1369), confirming its crystalline structure. However, upon modification with PEI, the characteristic peaks of SbW<sub>9</sub> disappeared in the SbW<sub>9</sub>@PEI composite, suggesting the interaction between SbW<sub>9</sub> and PEI leading to structural reorganization. The appearance of the wide and weak diffraction peak at ~28° (2θ) further indicated the formation of a non-crystalline composite.

The TGA curve of SbW<sub>9</sub>@PEI composite was shown in Fig. 1C. SbW<sub>9</sub>@PEI composite had three weight loss stages between 20 and 899 °C, with 1.97 % weight loss due to evaporation of crystalline water between 25 and 150 °C, 13.8 % from PEI decomposition between 150 and 580 °C, and 17.13 % from SbW<sub>9</sub> breakdown at >580 °C. The above results showed that the modification percentage of PEI was 13.8 %.

Table S1 presented the textural properties of SbW<sub>9</sub> and SbW<sub>9</sub>@PEI, including specific surface area, pore volume, and average particle size. SbW<sub>9</sub> had a specific surface area of 0.9490 m<sup>2</sup> g<sup>-1</sup>, pore volume of 0.00516 cm<sup>3</sup> g<sup>-1</sup>, and average particle size of 6322.23 nm. In contrast, SbW<sub>9</sub>@PEI exhibited a specific surface area of 18.2919 m<sup>2</sup> g<sup>-1</sup>, pore volume of 0.11416 cm<sup>3</sup> g<sup>-1</sup>, and average particle size of 328.01 nm. The larger specific surface area of SbW<sub>9</sub>@PEI suggested an interaction between SbW<sub>9</sub> and PEI.

The constituent elements and chemical states of SbW<sub>9</sub> and SbW<sub>9</sub>@PEI composite were analyzed using XPS (Fig. 2). The XPS survey spectrum of SbW<sub>9</sub> exhibited characteristic peaks corresponding to W4f, Sb3d, and O1s. The appearance of N1s peak in the spectrum of SbW<sub>9</sub>@PEI confirmed the successful modification of SbW<sub>9</sub> with PEI (Fig. 2A). In the Fig. 2B, the Sb 3d spectrum of SbW<sub>9</sub> showed peaks for Sb 3d3/2 and Sb 3d5/2 at 539.60 eV and 530.08 eV, indicating the +3 oxidation state of Sb. While, in the Sb 3d spectrum of SbW<sub>9</sub>@PEI, the peaks for Sb 3d3/2 and Sb 3d5/2 were observed at 538.60 eV and 529.40 eV, respectively, showing a slight energy decrease due to the interaction between SbW<sub>9</sub> and PEI. In the high-resolution N1s XPS spectrum (Fig. 2C), the peaks at 398.28 eV and 400.62 eV were attributed to C—N in the side chain and terminal amino group (C—NH<sub>3</sub><sup>+</sup>) of

PEI, respectively. The terminal amino groups could interact with negatively charged SbW<sub>9</sub> through electrostatic interactions. The high-resolution C1s XPS spectrum (Fig. 2D) of SbW<sub>9</sub>@PEI composite revealed C—C and C—N peaks at 284.8 eV and 286 eV, respectively.

The SEM and TEM images of SbW<sub>9</sub> and the SbW<sub>9</sub>@PEI composite were shown in the Fig. 3A–D. The SEM results indicated that SbW<sub>9</sub> exhibited a smooth, block-like structure with a relatively even surface. After surface modification with PEI, the SbW<sub>9</sub>@PEI composite was formed by the accumulation of numerous irregular round particles, resulting in a significantly altered morphology. The TEM results were similar to that of SEM. After modifying PEI, the surface of the composite became rough. The EDS results showed that SbW<sub>9</sub> was primarily made up of O, Na, W, and Sb, with percentages of 26.97 %, 14.74 %, 55 %, and 3.3 %. However, after PEI modification, the SbW<sub>9</sub>@PEI composite consisted of O, C, W, Sb and N, with contents of 20.12 %, 25.84 %, 44.66 %, 5.68 %, and 3.7 % (Table S2). The surface charge analysis indicated that the zeta potentials of SbW<sub>9</sub>@PEI were -4.02, -14.90 and -23.80 mV at pH 4, 7 and 11, respectively (Fig. S1). The above results demonstrated the successful modification of PEI onto the polyoxometalates SbW<sub>9</sub>.

### 3.2. Adsorption/recovery of proteins

#### 3.2.1. Protein adsorption behavior by SbW<sub>9</sub>@PEI

The adsorption behavior of SbW<sub>9</sub>@PEI composite was studied using two model proteins, Ova (pI 4.5) and Lys (pI 11.0). Firstly, the adsorption efficiency of Ova and Lys on SbW<sub>9</sub>@PEI was investigated at pH 4.0–11.0 (Fig. 4A). The adsorption efficiency of Ova reached 96 % at pH 4.0, gradually decreasing with increasing pH. This was because near the isoelectric point, the free —SH groups in Ova were well exposed (Xiong et al., 2024) and had an affinity with Sb in the composite, enhancing its adsorption. While, with increasing pH, Ova acquired a negative charge, resulting in reduced adsorption efficiency due to electrostatic repulsion with the composite. In contrast, Lys, which did not have the free —SH groups, exhibited low adsorption efficiency at pH 4.0. Therefore, at pH

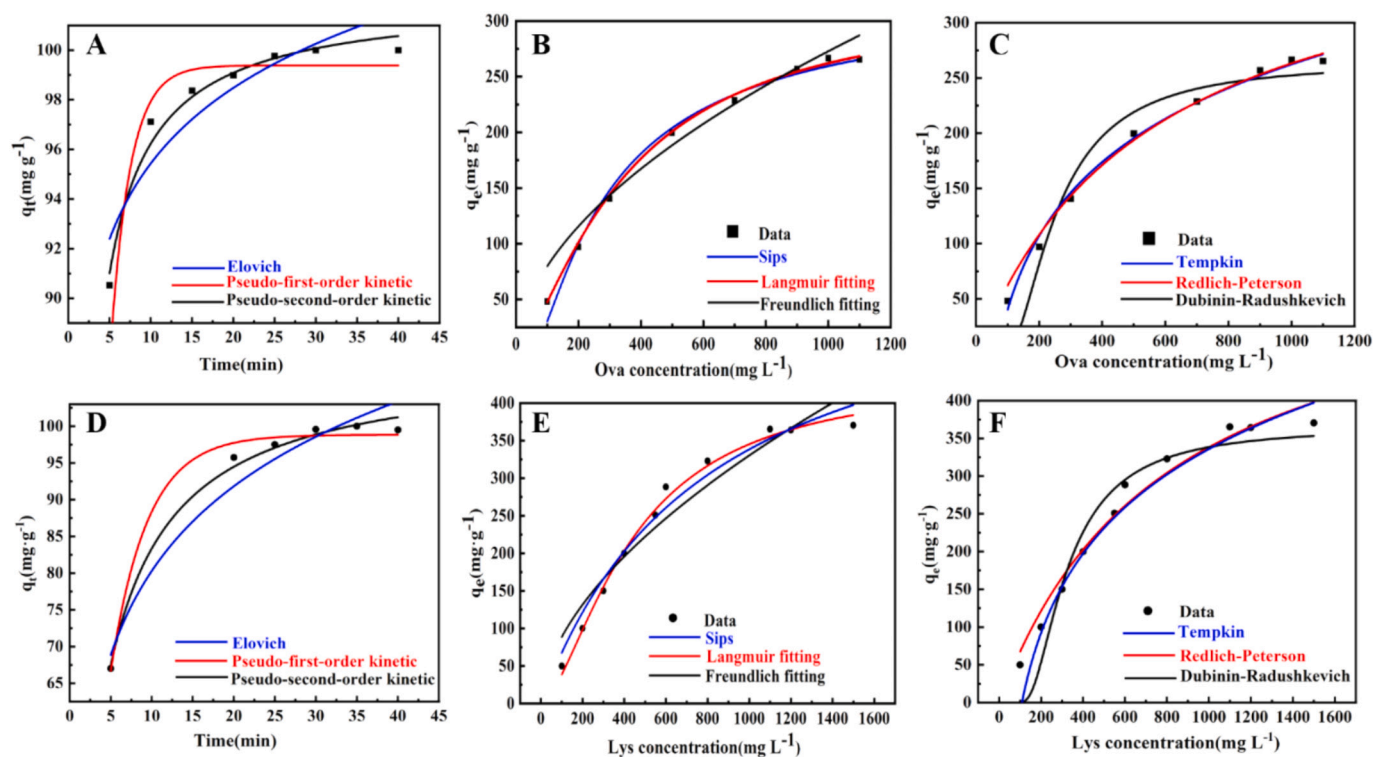


**Fig. 5.** (A) PFO, PSO and Elovich kinetics models for the Ova adsorption. (B) Sips, Langmuir and Freundlich isotherm models for the Ova adsorption. (C) Tempkin, Redlich, and Dubinin isotherm models for the Ova adsorption. (D) PFO, PSO and Elovich kinetics models for the Lys adsorption. (E) Sips, Langmuir and Freundlich isotherm models for the Lys adsorption. (F) Tempkin, Redlich and Dubinin isotherm models for the Lys adsorption.

4.0, the composite could selectively adsorb Ova. The adsorption efficiency of Lys gradually increased with the increase of pH in the range of 4.0–11.0, reaching 100 % at pH 11.0. At pH < 11, Lys become positively charged, leading to an increase in adsorption efficiency due to electrostatic interactions between the composite and Lys. At pH = 11, near the isoelectric point of Lys, the main driving force for adsorbing Lys onto the surface of the composite was the affinity force between exposed amino acid residues (such as Histidine molecules) on Lys molecules and Sb in the composite. The lysozyme surface had one His15 residue and two additional tryptophan residues at positions 62 and 123 (Li, Di, & Chen, 2002), which could coordinate with Sb due to their imidazole or indole groups. As the pH of the solution increased, the deprotonation of amino groups enhanced the affinity force. Furthermore, the affinity between Sb and aspartate residues at position 52 also contributed to the adsorption of Lys onto the composite surface (Li, 2005). On the other hand, Ova was negatively charged at pH 11, causing electrostatic repulsion with the negatively charged composite, resulting in low adsorption efficiency of Ova. Therefore, at pH 11, the composite could selectively adsorb Lys.

To further verify the adsorption selectivity of the composite towards Ova and Lys, the adsorption behavior of the composite towards three other proteins, namely ovomucoid (pI 4.1) and avidin (pI 10.0) which are both found in egg white, and bovine serum albumin (BSA, pI 4.9), like Ova, which belongs to the albumin family, was investigated. As shown in the results of Fig. 4A, at pH 4, the composite showed much lower adsorption efficiencies towards ovomucoid, avidin and BSA compared to Ova, due to the lack of free —SH groups in these proteins (Jain & Cheng, 2017; Qi et al., 2021; Rostamabadi et al., 2023). This indicated that the affinity between the free —SH groups in Ova and the composite was the main driving force for the selective adsorption of Ova. At pH 11, the adsorption efficiencies of ovomucoid, avidin and BSA were much lower than that of Lys, due to their negative charge causing electrostatic repulsion with composite. The results further demonstrated that the composite could effectively and controllably separate Ova and Lys.

The effect of adsorption time for the adsorption efficiency of Ova and Lys on composite were also studied. Fig. 4B showed that the adsorption efficiency of Ova and Lys increased gradually as the adsorption time increased. At 10 min, the adsorption efficiencies of both Ova and Lys reached their maximum values and subsequently entered a stable plateau phase. Further increasing the adsorption time had little impact on adsorption efficiency. Therefore, 10 min was chosen as the protein adsorption time for this experiment.

The impact of ionic strength on adsorption properties was investigated by adding varying amounts of NaCl to Ova and Lys solutions. Results were presented in Fig. 4C and D. For Ova adsorption at pH 4, the adsorption efficiency of SbW<sub>9</sub>@PEI composite for Ova and Lys remained constant as NaCl concentration increase (Fig. 4C). Under the condition of no salt addition, the adsorption efficiency of Ova on the surface of the composite was close to 100 %, and Ova exhibited significantly higher adsorption efficiency compared to Lys. The adsorption efficiency of Ova was shown to have little variation when the ionic strength was adjusted within a certain range. As a result, there was no need to alter the ionic strength when treating real biological samples in the following investigations. The adsorption efficiency of SbW<sub>9</sub>@PEI composite for Lys decreased with increasing NaCl concentration at pH 11, while the adsorption efficiency for Ova increased. The electrostatic attraction between Na<sup>+</sup> and the composite competed with lysozyme for adsorption, leading to a decrease in Lys adsorption efficiency with higher salt concentrations (Liu, Zhang, Chen, & Wang, 2011). The optimal adsorption condition for Lys was at 0 mol L<sup>-1</sup> NaCl concentration (Fig. 4D).

### 3.2.2. Adsorption kinetics and isotherms

Different adsorption kinetic models were adjusted to the experimental data of Ova and Lys. Estimated parameters, standard errors, and the correlation were presented in Table S3a and Table S4a. The curves of the fitted models were shown in Fig. 5A and D. The results showed that the adsorption kinetics of SbW<sub>9</sub>@PEI for Ova and Lys was well described

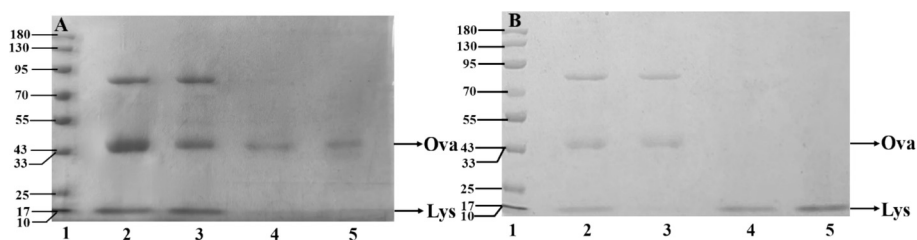


**Fig. 6.** SDS-PAGE assay results. (1 A) Protein Marker (kDa); (2 A) 300-fold diluted egg white without pretreatment; (3 A) 300-fold diluted egg white after adsorption by  $\text{SbW}_9\text{@PEI}$  composite; (4 A) Ova recovered from  $\text{SbW}_9\text{@PEI}$ ; (5 A) Ova standard solution of  $150 \mu\text{g mL}^{-1}$ ; (1B) Protein Marker (kDa); (2B) 300-fold diluted egg white without pretreatment; (3B) 300-fold diluted egg white after adsorption by  $\text{SbW}_9\text{@PEI}$  composite; (4B) Lys recovered from  $\text{SbW}_9\text{@PEI}$ ; (5B) Lys standard solution of  $150 \mu\text{g mL}^{-1}$ .

by the PSO model ( $R_{\text{Ova}}^2 = 0.97$  and  $R_{\text{Lys}}^2 = 0.99$ ), indicating a chemisorption process.

To further investigate the adsorption performance of  $\text{SbW}_9\text{@PEI}$  towards the target protein, the obtained adsorption data were fitted using the Sips, Langmuir, Freundlich, Tempkin, Redlich and Dubinin isotherm models. Table S3b and Table S4b presented the adjusted adsorption isotherm models along with estimated parameters, standard errors, and the correlation. The curves of the fitted models could be seen in Fig. 5B, C, E and F. The results revealed that when the Ova concentration exceeded  $1000 \mu\text{g mL}^{-1}$ , the adsorption capacity of Ova on the  $\text{SbW}_9\text{@PEI}$  composite remained stable, indicating that adsorption saturation had been achieved. The adsorption of Ova on the  $\text{SbW}_9\text{@PEI}$  surface followed a monolayer adsorption mechanism, which was well-described by the Langmuir model. A linear relationship was observed between  $C_e$  and  $C_e q_e^{-1}$ , with the equation  $y = 1.41468 \pm 0.00239x$  ( $R^2 = 0.991$ ), demonstrating a superior correlation compared to the other models (Fig. S2). Under optimal conditions, the theoretical maximum adsorption capacity of  $\text{SbW}_9\text{@PEI}$  for Ova was determined to be  $266.5 \text{ mg g}^{-1}$ .

When the concentration of Lys exceeded  $1500 \mu\text{g mL}^{-1}$ , the

adsorption capacity of the  $\text{SbW}_9\text{@PEI}$  composite for Lys remained stable, indicating saturation of adsorption (Fig. 5E and F) (Table S4b). The adsorption of Lys on the surface of the  $\text{SbW}_9\text{@PEI}$  was single-layer adsorption, fitting the Langmuir model. A linear relationship between  $C_e$  and  $C_e q_e^{-1}$  was observed, with the equation  $y = 0.63271 \pm 0.00223x$  and  $R^2 = 0.9917$ , showing better correlation than the other models (Fig. S3). The theoretical maximum adsorption capacity of Lys on the  $\text{SbW}_9\text{@PEI}$  composite under optimal conditions was  $366.3 \text{ mg g}^{-1}$ .

### 3.2.3. The recovery of the target proteins from the $\text{SbW}_9\text{@PEI}$ composite

To further investigate the structural properties of Ova and Lys adsorbed on  $\text{SbW}_9\text{@PEI}$ , the various stripping reagents were used for the elution of Ova and Lys, including CTAB ( $0.01 \text{ mol L}^{-1}$ ), BR buffer (pH 4.0 and 11.0), Tris-HCl ( $2 \text{ mol L}^{-1}$ , pH 9.0), NaCl ( $0.1 \text{ mol L}^{-1}$ ),  $\text{Na}_2\text{HPO}_4$  ( $0.01 \text{ mol L}^{-1}$ ), and SDS ( $0.1 \text{ mol L}^{-1}$ ). As illustrated in Fig. S4, Tris-HCl ( $2 \text{ mol L}^{-1}$ , pH 9.0) and CTAB ( $0.01 \text{ mol L}^{-1}$ ) exhibited the most effective elution for Ova and Lys, respectively, achieving elution efficiencies of 93.9 % and 93.2 %. The superior elution performance of Tris-HCl could be attributed to the abundance of hydroxyl groups in its structure, which facilitated hydrogen bonding with the oxygen atoms on

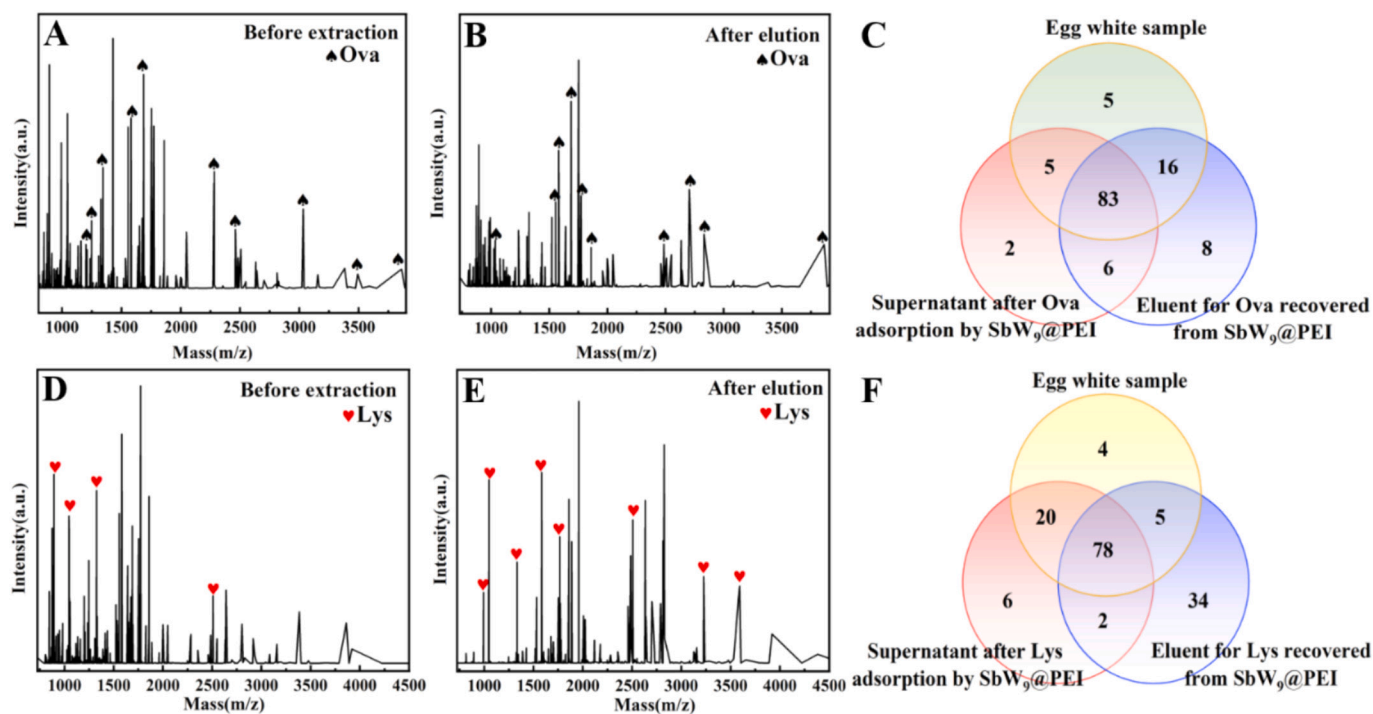


**Fig. 7.** LC-MS/MS analysis results. (A) 300-fold diluted egg white without pretreatment; (B) Ova recovered from  $\text{SbW}_9\text{@PEI}$ ; (C) Venn diagram of the distribution of protein species in 300-fold diluted egg white without pretreatment, the supernatant after Ova adsorption by  $\text{SbW}_9\text{@PEI}$  composite and eluent for Ova recovered from  $\text{SbW}_9\text{@PEI}$ ; (D) 300-fold diluted egg white without pretreatment; (E) Lys recovered from  $\text{SbW}_9\text{@PEI}$ ; (F) Venn diagram of the distribution of protein species in 300-fold diluted egg white without pretreatment, the supernatant after Lys adsorption by  $\text{SbW}_9\text{@PEI}$  composite and eluent for Lys recovered from  $\text{SbW}_9\text{@PEI}$ .

**Table 1**

Table 1 The 34 low-abundance proteins in the Lys elution from egg white using SbW<sub>9</sub>@PEI composite as an adsorbent.

Protein names	Sequence
40S ribosomal protein S8 (Fragment)	IIDVVYNASNNELVR
60 kDa heat shock protein	KPLVIAEDVDGEALSTLVLNR
Beta-enolase	ISVVEQEK
Calmodulin	VFDKDGNGYISAAELR
Carbamoyl-phosphate synthase 1	VLLGSGGLSIGQAGEFDYSGQAVK
Catalase	GPLLVDVVFTDEMAHFDR
Endoplasmic reticulum chaperone	LISLTDENALAGNEELTVK
Enhancer of rudimentary homolog	SHTILLVQPTKRPEGR
Epiplakin 1	IITEETMEK
Fibronectin	LGVRPSQGGEAPR
Glyceraldehyde-3-phosphate dehydrogenase	VPTPNVSVVDLTCR
Heteroous nuclear ribonucleoprotein H1	VTGEADVEFATHEDAVAAMSK
Heteroous nuclear ribonucleoprotein H3	ATGEADVEFVTHEDAVAAMSK
Heat shock protein 90 (Fragment)	VILHLKEDQTEYLEER
Large ribosomal subunit protein uL2	TELFIAAEGIHGTQFVYCGKK
Large ribosomal subunit protein uL23	KIEDNNTLVFIVDVK
Mitochondrial-processing peptidase subunit alpha	MAAAVAWLR
Non-selective voltage-gated ion channel VDAC1	TDEFQLHTNVNDGTEFGGSYQK
NudC domain containing 3	MGAAGLSQSWLR
Outer dense fiber protein 2	LEITPPESEKMMSVLR
Phosphopyruvate hydratase	SKFGANAILGVSLAVCK
Programmed cell death 6 interacting protein	LQHAADLVK
Prohibitin-2	AKDFSLLDDVAITELSFRR
Proliferation-associated 2G4	AEFEVHEVYAVDVLVSSGEGK
Proton-translocating NAD (P)(+) transhydrogenase	VLIIGGGVAGLASAGAAK
Pyruvate kinase PKM	LDIDSEPTIAR
Ribosomal protein L11	KNNFSDTGNFGFIQEHIDLGK
RNA helicase (Fragment)	TATFAISLLQLEIDLK
Small ribosomal subunit protein uS12	KITAFVPPNDGCLNFIEENDEVLVAGFR
Splicing factor 3a subunit 1	TQQAAQANITLQEQIEAIHK
Stress-70 protein	GVPQIEVTFDIDANGIVHVS AK
Triosephosphate isomerase	VVFEQTK
Tubulin alpha chain	AYHEQLSVAEITNACFEPANQMVK
Tubulin beta chain	VSDTVVEPYNATLSVHQLVENTDETYCIDNEALYDICFR

the polyoxometalates composite, thereby enabling the efficient release of Ova from the SbW<sub>9</sub>@PEI surface (Chen et al., 2015; Xu, Cao, Lin, Shu, & Wang, 2021). On the other hand, CTAB, a surfactant containing hydrophobic groups, possessed a (CH<sub>3</sub>)<sub>3</sub>-N<sup>+</sup>-(CH<sub>2</sub>)CH<sub>3</sub> cation that could form electrostatic interactions with the composite and the interaction was likely responsible for CTAB's optimal elution effect on Lys (Khan et al., 2019; Zhang, Guo, Hu, Chen, & Wang, 2017).

### 3.2.4. The reusability of the SbW<sub>9</sub>@PEI composite

The reusability of the SbW<sub>9</sub>@PEI composite is crucial in practical applications. The results in Fig. S5 showed that after six adsorption and desorption cycles, the adsorption efficiency of the composite for Ova and Lys remained above 80 %. The findings demonstrated the good reusability of the composite for separating and purifying Ova and Lys.

### 3.3. Isolation of Ova and Lys from egg white by the SbW<sub>9</sub>@PEI

The practicality of the SbW<sub>9</sub>@PEI composite was confirmed by successfully separating and purifying Lys and Ova from egg white. The egg white was processed according to the method described in Section 2.5 and the obtained Lys and Ova elution was immediately analyzed by SDS-PAGE and LC-MS/MS. The results of SDS-PAGE analysis were presented in Fig. 6A and B. In Fig. 6A, Lane 1 showed protein molecular weight markers ranging from 10 to 180 kDa. Lane 2 displayed a 300-fold diluted egg white sample, with protein bands corresponding to Ovt (77.7 kDa), Ova (44.3 kDa), and Lys (14.3 kDa). Lane 3 represented the supernatant after adsorption by SbW<sub>9</sub>@PEI, where the band of Ova at 44.3 kDa decreased significantly. Lane 4 showed the supernatant after elution with a Tris-HCl (2 mol L<sup>-1</sup>, pH 9.0) solution, displaying a distinct Ova band at 44.3 kDa. In Fig. 6B, Lane 1 and Lane 2 was similar to that of Fig. 6A. Lane 4 illustrated the supernatant after elution with 0.01 mol L<sup>-1</sup> CTAB, showing a single band at 14.3 kDa, consistent with the standard Lys band in Lane 5. These results indicated that the SbW<sub>9</sub>@PEI composite was capable of effectively separating and purifying Ova and Lys with high-purity from complex biological samples-egg white under controlled pH conditions.

LC-MS/MS analysis (Fig. 7) was conducted on the original egg white sample, the supernatant after adsorption, and the protein eluent to validate the performance of the SbW<sub>9</sub>@PEI composite in purifying Ova and Lys for potential proteomics applications. The results showed that original egg white sample showed multiple interfering proteins (Fig. 7A and D). However, after solid-phase extraction with SbW<sub>9</sub>@PEI, the interfering proteins' signal peaks were significantly reduced or even disappeared, indicating the high selectivity of SbW<sub>9</sub>@PEI for Ova and Lys (Fig. 7B and E). In addition, for Ova adsorption, a total of 96 and 113 proteins were identified in the supernatant after adsorption and the eluent, respectively including 2 and 8 proteins not found in the original sample, which led to the identification of 10 low-abundance proteins (Fig. 7C). Similarly, 106 and 119 proteins were identified in the supernatant after adsorption and the Lys eluent, respectively including 6 and 34 additional proteins (Table 1) not present in the original sample, which contributed to the detection of 40 low-abundance proteins (Fig. 7F). The results showed the changes in protein composition during the separation and purification process, highlighting the excellent performance of SbW<sub>9</sub>@PEI in separating Ova and Lys.

## 4. Conclusions

A new polyoxometalates composite (SbW<sub>9</sub>@PEI) was successfully created using a simple liquid-phase method at room temperature. This composite had pH-responsive selectivity, allowing for effective and controlled separation of Ova and Lys directly from complex egg white sample. At pH 4.0, the composite (2 mg) achieved the 96 % adsorption efficiency for Ova (100 µg mL<sup>-1</sup>, 1 mL), with the adsorption capacity of 266.5 mg g<sup>-1</sup>. At pH 11.0, it exhibited 100 % adsorption efficiency for Lys (100 µg mL<sup>-1</sup>, 1 mL), with the adsorption capacity of 366.3 mg g<sup>-1</sup>. SDS-PAGE and LC-MS/MS analyses confirmed the high purity of the separated proteins. Notably, compared with untreated egg white, 10 and 40 low-abundance proteins were respectively identified through the separation of Ova and Lys, showcasing the composite's ability to enrich and detect trace proteins. However, the performance of the composite in other more complex biological samples may be challenged by interfering species such as many coexisting proteins, polysaccharides, or salt ions that induce competitive binding at adsorption sites, thereby compromising separation efficiency and specificity and necessitates further in-depth research. Building on the findings of this study, rigorous scientific experiments can be devised to progressively broaden the application range of the composite. In conclusion, the composite with pH-responsive selectivity holds great potential for diverse applications. This study expands the use of polyoxometalates in life science separations, offering a promising platform for functional food development, food safety and

more through precise protein purification. In the future, integrating technologies such as biomimetic recognition, multi-dimensional screening, and artificial intelligence optimization will enhance the separation and purification performance of polyoxometalates composite, enabling the precise capture of specific proteins in complex biological samples.

### CRedit authorship contribution statement

**Qian Sun:** Writing – original draft, Methodology, Formal analysis, Data curation. **Yujing Wang:** Investigation, Data curation. **Ye Wang:** Visualization, Investigation. **Guangtian Zhu:** Visualization, Investigation. **Yifei Niu:** Visualization, Investigation. **Weizhu Wang:** Investigation. **Ronghua Fan:** Validation, Supervision. **Dandan Zhang:** Writing – review & editing, Validation, Supervision.

### Declaration of competing interest

The authors declare that they have no known competing financial interests or personal relationships that could have appeared to influence the work reported in this paper.

### Acknowledgments

This study was supported by the National Natural Science Foundation of China (22304123), Science and Technology Innovation Team Project of Liaoning Provincial Department of Education (LJ222410164015), Science and Technology Innovation Fund for graduate students of Shenyang Medical College (Y20240518) and Student Research Project of Shenyang Medical College (20249018).

### Appendix A. Supplementary data

Supplementary data to this article can be found online at <https://doi.org/10.1016/j.foodchem.2025.146122>.

### Data availability

Data will be made available on request.

### References

- Bilkova, Z., Shabani, E., Moravek, O., Korecka, L., Slovakova, M., & Jankovicova, B. (2025). Fundamentals of protein affinity chromatography: How to prepare and properly use an affinity matrix. *Journal of Chromatography A*, 1756, Article 466061. <https://doi.org/10.1016/j.chroma.2025.466061>
- Bösing, M., Loose, I., Pohlmann, H., & Krebs, B. (2006). New strategies for the generation of large Heteropolymetalate clusters: The  $\beta$ -B-SbW<sub>9</sub> fragment as a multifunctional unit. *Chemistry-A European Journal*, 3(8), 1232–1237. <https://doi.org/10.1002/chem.19970030810>
- Cai, J., Ye, R., Liu, X., Guo, L., & Qiao, X. (2020). Ionic strength effect on regulating the synthetic assembly of polyoxometalate clusters with slow magnetic relaxation behavior. *Dalton Transactions*, 49(46), 16954–16961. <https://doi.org/10.1039/d0dt02409k>
- Chen, Q., Zhang, D.-D., Wang, M.-M., Chen, X.-W., & Wang, J.-H. (2015). A novel organic-inorganic hybrid polyoxometalate for the selective adsorption/isolation of  $\beta$ -lactoglobulin. *Journal of Materials Chemistry B*, 3(34), 6964–6970. <https://doi.org/10.1039/c5tb01298h>
- D’Incecco, P., Gatti, M., Hogenboom, J. A., Bottari, B., Rosi, V., Neviani, E., & Pellegrino, L. (2016). Lysozyme affects the microbial catabolism of free arginine in raw-milk hard cheeses. *Food Microbiology*, 57, 16–22. <https://doi.org/10.1016/j.fm.2015.11.020>
- Dobson, D. E., Prager, E. M., & Wilson, A. C. (1984). Stomach lysozymes of ruminants. I. Distribution and catalytic properties. *Journal of Biological Chemistry*, 259(18), 11607–11616. [https://doi.org/10.1016/s0021-9258\(18\)90907-5](https://doi.org/10.1016/s0021-9258(18)90907-5)
- Gazme, B., Rezaei, K., & Udenigwe, C. C. (2022). Epitope mapping and the effects of various factors on the immunoreactivity of main allergens in egg white. *Food & Function*, 13(1), 38–51. <https://doi.org/10.1039/d1fo01867a>
- Gong, P., Wang, Y., Zhao, J., & Yang, G.-Y. (2024). Antimonotungstate-based heterometallic framework formed by the synergistic strategy of in situ-generated Krebs-type building units and the substitution reaction and its high-efficiency biosensing KRAS gene. *Inorganic Chemistry*, 64(1), 315–326. <https://doi.org/10.1021/acs.inorgchem.4c04589>
- Han, Z.-G., Zhang, H.-X., Zhang, D.-S., Liu, C.-N., Zheng, R., Xia, G.-B., & Wang, X.-X. (2016). Sandwich-type Polyoxotungstate consisting of two different Trilacunary Keggin-type units. *Inorganic Chemistry*, 55(24), 12488–12491. <https://doi.org/10.1021/acs.inorgchem.6b01848>
- Jain, A., & Cheng, K. (2017). The principles and applications of avidin-based nanoparticles in drug delivery and diagnosis. *Journal of Controlled Release*, 245, 27–40. <https://doi.org/10.1016/j.jconrel.2016.11.016>
- Khan, J. M., Malik, A., Ahmed, A., Rehman, M. T., AlAjmi, M. F., Khan, R. H., ... Abdullah, E. M. (2019). Effect of cetyltrimethylammonium bromide (CTAB) on the conformation of a hen egg white lysozyme: A spectroscopic and molecular docking study. *Spectrochimica Acta Part A: Molecular and Biomolecular Spectroscopy*, 219, 313–318. <https://doi.org/10.1016/j.saa.2019.04.062>
- Li, F., Hu, X., Sa, R., & Feng, J. (2014). Receding mechanism of NLO response of polyanion [M<sub>6</sub>O<sub>26</sub>]<sup>4-</sup> (M = Cr, Mo, W) and the closed loops theory analysis. *New Journal of Chemistry*, 38(6), 2619–2628. <https://doi.org/10.1039/c3nj01511d>
- Li, R., Di, Z., & Chen, G. (2002). Interaction between immobilized metal and protein in metal chelate affinity chromatography. *Chinese Journal of Analytical Chemistry*, 30(5), 552–555.
- Li, S. J. (2005). Structural details at active site of hen egg white lysozyme with di- and trivalent metal ions. *Biopolymers*, 81(2), 74–80. <https://doi.org/10.1002/bip.20367>
- Liu, J. W., Zhang, Q., Chen, X. W., & Wang, J. H. (2011). Surface assembly of graphene oxide nanosheets on SiO<sub>2</sub> particles for the selective isolation of Hemoglobin. *Chemistry-A European Journal*, 17(17), 4864–4870. <https://doi.org/10.1002/chem.201003361>
- Liu, L., Chen, H., Wang, Y., Cheng, W., He, J., Xiao, F., & Li, S. (2025). Characterization of quercetin-ovalbumin complexes stabilizing emulsions: A perspective on the complex binding mechanism. *International Journal of Biological Macromolecules*, 307. <https://doi.org/10.1016/j.ijbiomac.2025.141970>
- Liu, S., Li, Z., Yu, B., Wang, S., Shen, Y., & Cong, H. (2020). Recent advances on protein separation and purification methods. *Advances in Colloid and Interface Science*, 284, Article 102254. <https://doi.org/10.1016/j.cis.2020.102254>
- Lv, R., Zhang, X., Sun, R., Chen, L., Zhang, Y., Sheng, R., ... Qi, Y. (2022). Hierarchical micro-nanostructures from polyoxometalates and polydopamine: Characterization, electrochemical and intrinsic peroxidase-like properties. *Particuology*, 64, 178–185. <https://doi.org/10.1016/j.partic.2021.07.004>
- Niu, X., Zhu, L., Xi, L., Guo, L., & Wang, H. (2020). An antimicrobial agent prepared by N-succinyl chitosan immobilized lysozyme and its application in strawberry preservation. *Food Control*, 108, Article 106829. <https://doi.org/10.1016/j.foodcont.2019.106829>
- Omwoma, S., Gore, C. T., Ji, Y., Hu, C., & Song, Y.-F. (2015). Environmentally benign polyoxometalate materials. *Coordination Chemistry Reviews*, 286, 17–29. <https://doi.org/10.1016/j.ccr.2014.11.013>
- Qi, X., Xu, D., Zhu, J., Wang, S., Peng, J., Gao, W., & Cao, Y. (2021). Studying the interaction mechanism between bovine serum albumin and lutein dipalmitate: Multi-spectroscopic and molecular docking techniques. *Food Hydrocolloids*, 113, Article 106513. <https://doi.org/10.1016/j.foodhyd.2020.106513>
- Rao, S., Xu, G., Lu, X., Zhang, R., Gao, L., Wang, Q., ... Jiao, X. (2020). Characterization of ovalbumin-carvacrol inclusion complexes as delivery systems with antibacterial application. *Food Hydrocolloids*, 105, Article 105753. <https://doi.org/10.1016/j.foodhyd.2020.105753>
- Rostamabadi, H., Chaudhary, V., Chhikara, N., Sharma, N., Nowacka, M., Demirkesen, I., ... Falsafi, S. R. (2023). Ovalbumin, an outstanding food hydrocolloid: Applications, technofunctional attributes, and nutritional facts, A systematic review. *Food Hydrocolloids*, 139, Article 108514. <https://doi.org/10.1016/j.foodhyd.2023.108514>
- Salazar Marcano, D. E., Lentink, S., Moussawi, M. A., & Parac-Vogt, T. N. (2021). Solution dynamics of hybrid Anderson-Evans polyoxometalates. *Inorganic Chemistry*, 60(14), 10215–10226. <https://doi.org/10.1021/acs.inorgchem.1c00511>
- Sun, Y., Li, H., Zou, Y., Ma, P., Niu, J., & Wang, J. (2023). A Hexameric ruthenium(III)-containing Tungstoantimonate with good proton conductivity performance. *Inorganic Chemistry*, 62(35), 14142–14146. <https://doi.org/10.1021/acs.inorgchem.3c01342>
- Taheri, M. (2021). Polyoxometalates and metal-organic frameworks based dual-functional catalysts for detoxification of bis(2-chloroethyl) Sulfide and organophosphorus agents. *Catalysis Surveys from Asia*, 26(1), 1–15. <https://doi.org/10.1007/s10563-021-09347-3>
- Wang, C., Yang, M., Wang, X., Ma, H., Tian, Y., Pang, H., ... Gao, K. (2022). Hierarchical CoS<sub>2</sub>/MoS<sub>2</sub> flower-like heterostructured arrays derived from polyoxometalates for efficient electrocatalytic nitrogen reduction under ambient conditions. *Journal of Colloid and Interface Science*, 609, 815–824. <https://doi.org/10.1016/j.jcis.2021.11.087>
- Wang, Z. L., Tang, X., Wang, M., She, Y. X., Yang, B. R., Sheng, Q. H., & Abd El-Aty, A. M. (2024).  $\beta$ -Lactoglobulin separation from whey protein: A comprehensive review of isolation and purification techniques and future perspectives. *Journal of Dairy Science*, 107(12), 11785–11795. <https://doi.org/10.3168/jds.2024-25321>
- Xiong, Z., Weng, T., Wang, J., Xiao, S., Suo, H., & Li, D. (2024). Regulatory mechanisms of phosphorylation in ovalbumin self-assembly for aggregates formation: Insights into size, structure, and morphology. *Food Hydrocolloids*, 157, Article 110431. <https://doi.org/10.1016/j.foodhyd.2024.110431>
- Xu, W., Cao, J.-F., Lin, Y.-N., Shu, Y., & Wang, J.-H. (2021). Functionalized polyoxometalate microspheres ensure selective adsorption of phosphoproteins and glycoproteins. *Chemical Communications*, 57(27), 3367–3370. <https://doi.org/10.1039/d1cc00325a>
- Yan, Y., Li, B., He, Q., He, Z., Ai, H., Wang, H., ... Wu, L. (2012). Synthesis and redox-responsive self-assembly of ferrocene grafted Anderson-type polyoxometalate hybrid complexes. *Soft Matter*, 8(5), 1593–1600. <https://doi.org/10.1039/c1sm06610b>

- Yang, T., & Yan, W. (2025). Strategies for enhancing the antibacterial efficacy of lysozyme and the resulting outcome. *International Journal of Biological Macromolecules*, 310, Article 142137. <https://doi.org/10.1016/j.ijbiomac.2025.143137>
- Zhang, D.-D., Guo, P.-F., Hu, L.-L., Chen, X.-W., & Wang, J.-H. (2017). Regulation of the adsorption selectivity of acidic or basic proteins using a polyoxometalate composite. *Journal of Materials Chemistry B*, 5(4), 750–756. <https://doi.org/10.1039/c6tb02733d>
- Zhang, D.-D., Guo, Z.-Y., Guo, P.-F., Hu, X., Chen, X.-W., & Wang, J.-H. (2018). Polyoxometalate-coated magnetic nanospheres for highly selective isolation of immunoglobulin G. *ACS Applied Materials & Interfaces*, 10(26), 21876–21882. <https://doi.org/10.1021/acsami.8b05334>
- Zhang, W., Liu, S., Feng, D., Zhang, C., Sun, P., & Ma, F. (2009). Two novel Krebs-type polyoxoanions  $[\text{Cu}_2(\text{WO}_2)_2(\beta\text{-XW}_9\text{O}_{33})_2]^{12-}$  (X=Sb<sup>III</sup>, Bi<sup>III</sup>) resulting in 2D layer structures linked by copper(I) ions and copper(II) complex groups. *Journal of Molecular Structure*, 936(1–3), 194–198. <https://doi.org/10.1016/j.molstruc.2009.07.038>